PERGAMON

Journal of Structural Geology 24 (2002) 783–796

JOURNAL OF STRUCTURAL GEOLOGY

www.elsevier.com/locate/jstrugeo

Kinematics of a growth fault/raft system on the West African margin using 3-D restoration

Delphine Rouby[a,*], Stéphane Raillard[b], François Guillocheau[a], Renaud Bouroullec[c], Thierry Nalpas[a]

[a]*Géosciences Rennes, UMR 6118 CNRS, Campus de Beaulieu, 35042 Rennes Cédex, France*
[b]*TotalFinaElf, Avenue Larribau, 64018 Pau Cédex, France*
[c]*Imperial College, Prince Consort Road, London SW7 2BP, UK*

Received 24 February 2000; revised 24 January 2001; accepted 1 June 2001

Abstract

The ability to quantify the movement history associated with growth structures is crucial in the understanding of fundamental processes such as the growth of folds or faults in 3-D. In this paper, we present an application of an original approach to restore in 3-D a listric growth fault system resulting from gravity-induced extension located on the West African margin. Our goal is to establish the 3-D structural framework and kinematics of the study area. We construct a 3-D geometrical model of the fault system (from 3-D seismic data), then restore six stratigraphic surfaces and reconstruct the 3-D geometry of the system at six incremental steps of its history.

The evolution of the growth fault/raft system corresponds to the progressive separation of two rafts by regional extension, resulting in the development of an intervening basin located between them that evolved in three main stages: (1) the rise of an evaporite wall, (2) the development of a symmetric basin as the elevation of the diapir is reduced and buried, and (3) the development of asymmetric basins related to two systems of listric faults (the main fault F1 and the graben located between the rollovers and the lower raft).

Important features of the growth fault/raft system could only be observed in 3-D and with increments of deformation restored. The rollover anticline (associated with the listric fault F1) is composed of two sub-units separated by an E–W oriented transverse graben indicating that the displacement field was divergent in map view. The rollover units are located within the overlap area of two fault systems and displays a 'mock-turtle' anticline structure. The seaward translation of the lower raft is associated with two successive vertical axis rotations in the opposite sense (clockwise then counter-clockwise by about 10°). This results from the fact that the two main fault systems developed successively. Fault system F1 formed during the Upper Albian, and the graben during the Cenomanian.

Using a new approach of 3-D restoration, this study suggests a consistent solution for: (1) the processes of deformation of a fault system, (2) the faulting kinematics, and (3) the incremental steps of deformation.

Keywords: Kinematics; Growth fault/raft systems; Gravity-induced extension

1. Introduction

Growth fault systems, that is faults that develop when sediments are being deposited, are key elements in understanding deformation processes in 3-D. Indeed, successively deposited sedimentary layers are involved in the different stages of the growth of the structure and produce a record of the deformation history.

There are two mechanisms by which faults can grow: propagation of fault tips or linkage with other faults that may or may not be kinematically related (see review by Cowie, 1998). Geometric characteristics of growth fault systems (e.g. ratio of fault length to maximum offset, segmentation, vertical or lateral relays, strike changes resulting from linkage) depend upon the balance between these fault growth mechanisms and how they change with time. However, sedimentation may also have a significant impact on both the geometry and the kinematics of structures (e.g. Vendeville et al., 1987; Vendeville and Cobbold, 1987, 1988; Merle and Abidi, 1995; Tondji-Biyo, 1995; Mauduit and Brun, 1998; Nalpas et al., 1999).

The ability to quantify the movement history associated with growth structures can provide a fundamental insight into the processes of growth of folds and faults, their kinematics, and interactions. Our approach is to measure the displacements associated with a growth fault by restoring several stratigraphic surfaces in syn-tectonic deposits, i.e. reconstructing their undeformed geometry. The difference between the deformed (current) and undeformed (restored)

* Corresponding author. Tel.: +33-2-2323-5771; fax: +33-2-2323-6100.
E-mail address: Delphine.Rouby@univ-rennes1.fr (D. Rouby).

0191-8141/02/$ - see front matter
PII: S0191-8141(01)00108-0

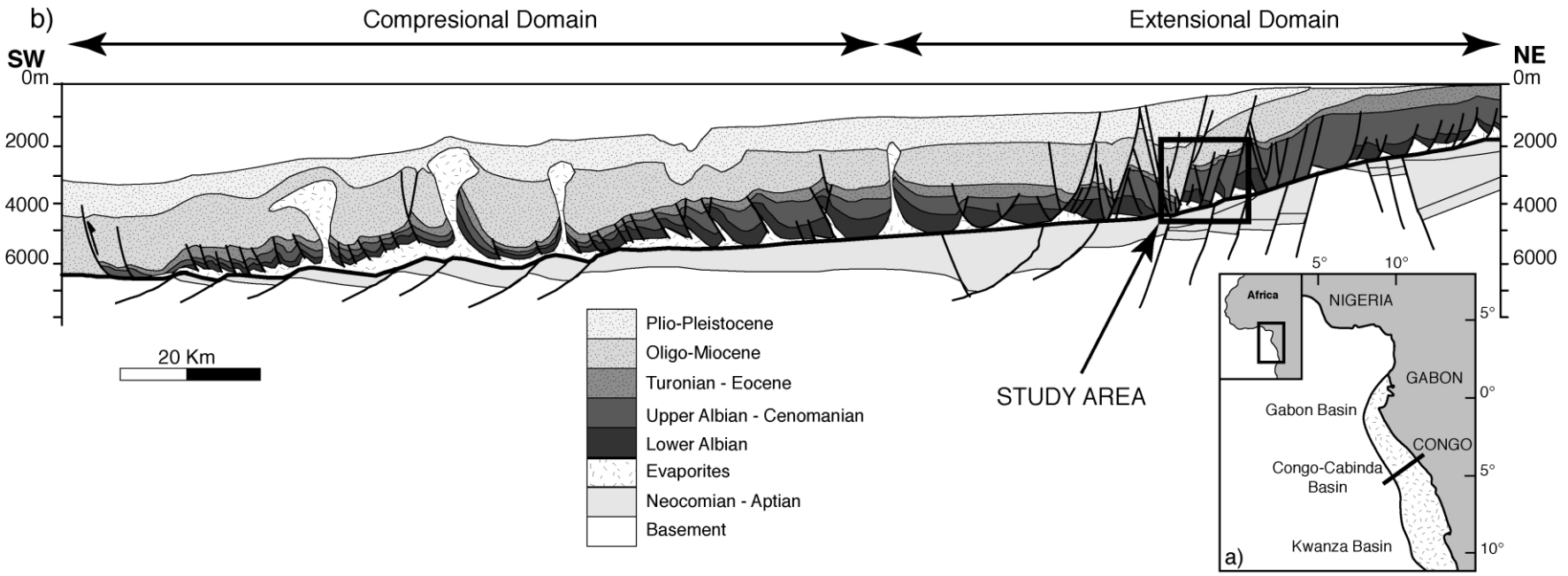

Fig. 1. (a) Location of the sedimentary basins off the coasts of Gabon and Congo (modified after Curie, 1984). Dashed area shows the extent of salt basins. (b) Synthetic cross-section across the Congo Cabinda Basin. Approximate location shown in (a). The outlined box indicates the study area.

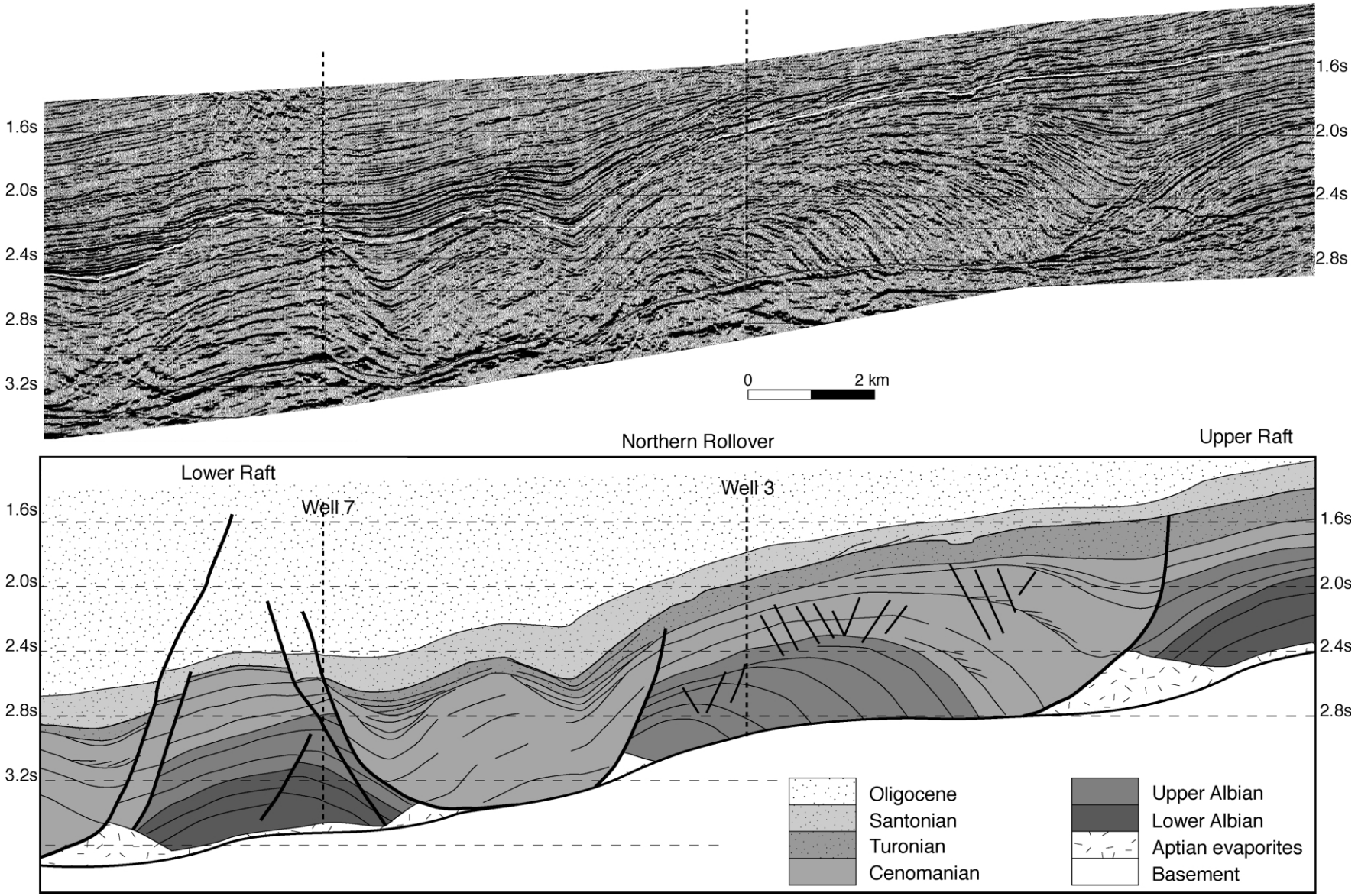

Fig. 2. Line drawing of an E–W seismic cross-section (see text for explanation).

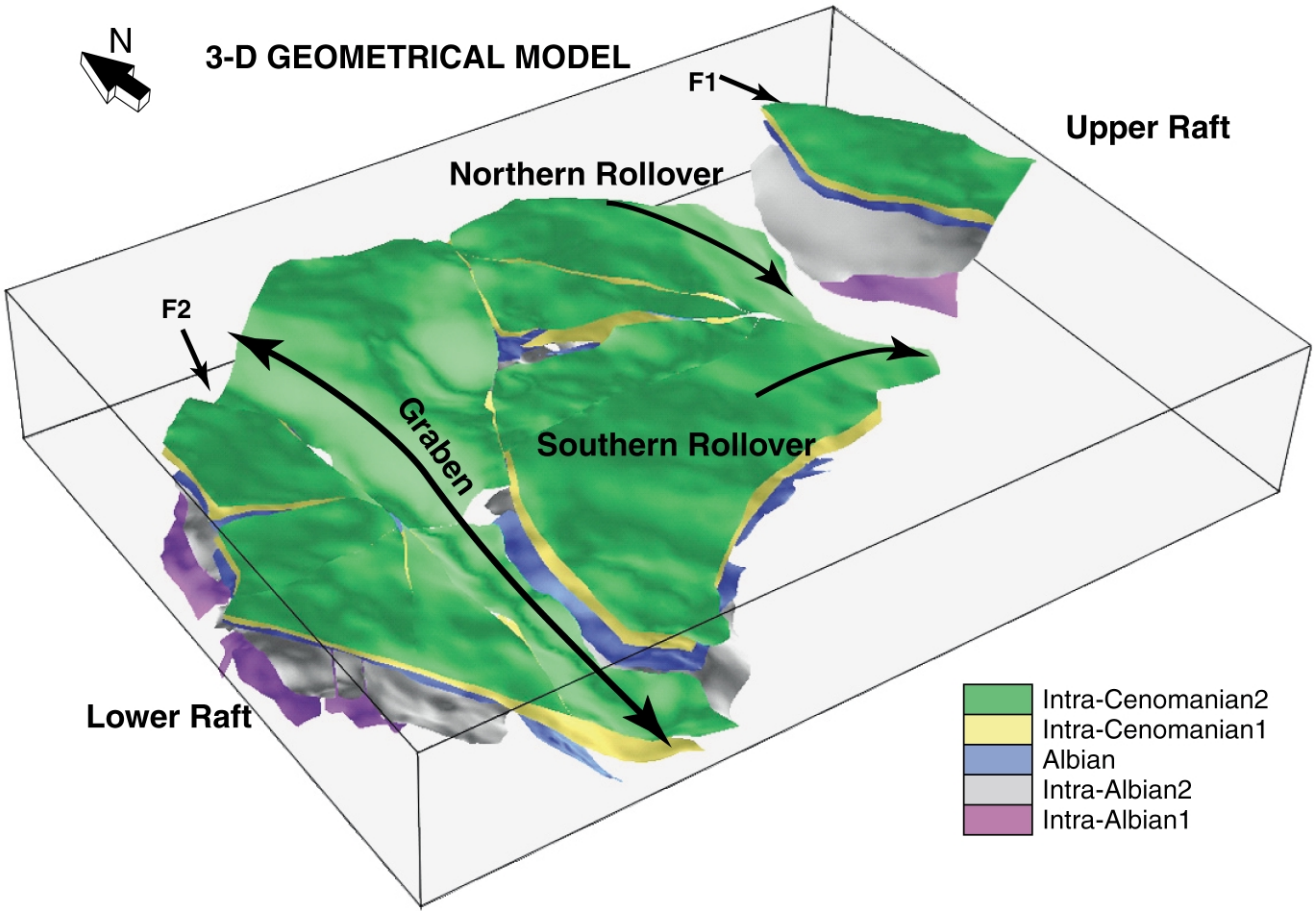

Fig. 3. 3-D view of the geometrical model with five stratigraphic surfaces (Intra-Albian1, Intra-Albian2, Albian, Intra-Cenomanian1 and Intra-Cenomanian2). Note the upper and lower raft, separated by the rollover anticlines (northern and southern) and the graben.

states gives the field of finite displacements. Recent techniques allow the reconstruction to be performed in 3-D taking into account folds and/or faults (Gratier et al., 1991; Guillier, 1991; Gratier and Guillier, 1993; Samson, 1996; Williams et al., 1997; Rouby et al., 2000). This is an important methodological step since the growth of faults is fundamentally a 3-D process.

In this paper, we present an application of a new approach of 3-D restoration proposed by Rouby et al. (2000) to a raft/listric fault system resulting from gravity-induced extension located on the West African margin. Our goal is to establish the 3-D structural framework and kinematics of the study area.

First, we present the 3-D geometrical model of the fault system (established from 3-D seismic data). We then restore six stratigraphic surfaces of the model and reconstruct the 3-D geometry of the system at six incremental steps of its history.

2. Geological setting

The studied area is located along the West African margin, in the Congo–Cabinda Basin (Fig. 1). One of the main tectonic features of the West African passive margin is the gravitational spreading of post-rift sediments above a décollement layer made up of Aptian evaporites (e.g. Duval et al., 1992; Lundin, 1992; Liro and Coen, 1995; Spathopoulos, 1996). In the studied area, gravity-driven tectonics initiated during the Albian and persisted throughout the Cenozoic. This created two structural domains each about 100 km wide, an upper extensional domain and its compressive toe located downslope (Fig. 1). The extensional domain is locally associated with a massive amount of thin-skinned extension (over 400%) of the overburden, creating rafts of allochtonous fault blocks that are no longer in contact (e.g. Burollet, 1975; Duval et al., 1992). The studied area is a growth fault/raft system, about 15 km wide, located within the extensional domain (Fig. 1).

We focus here on the Albo–Cenomanian history of the structure because most of the displacement on the faults in the study area occurred before the Oligocene (Fig. 1). Lower Albian sediments are represented by a shallow water, mixed carbonate platform prograding onto the Aptian evaporites. During the Upper Albian, it is covered by outer shelf shale

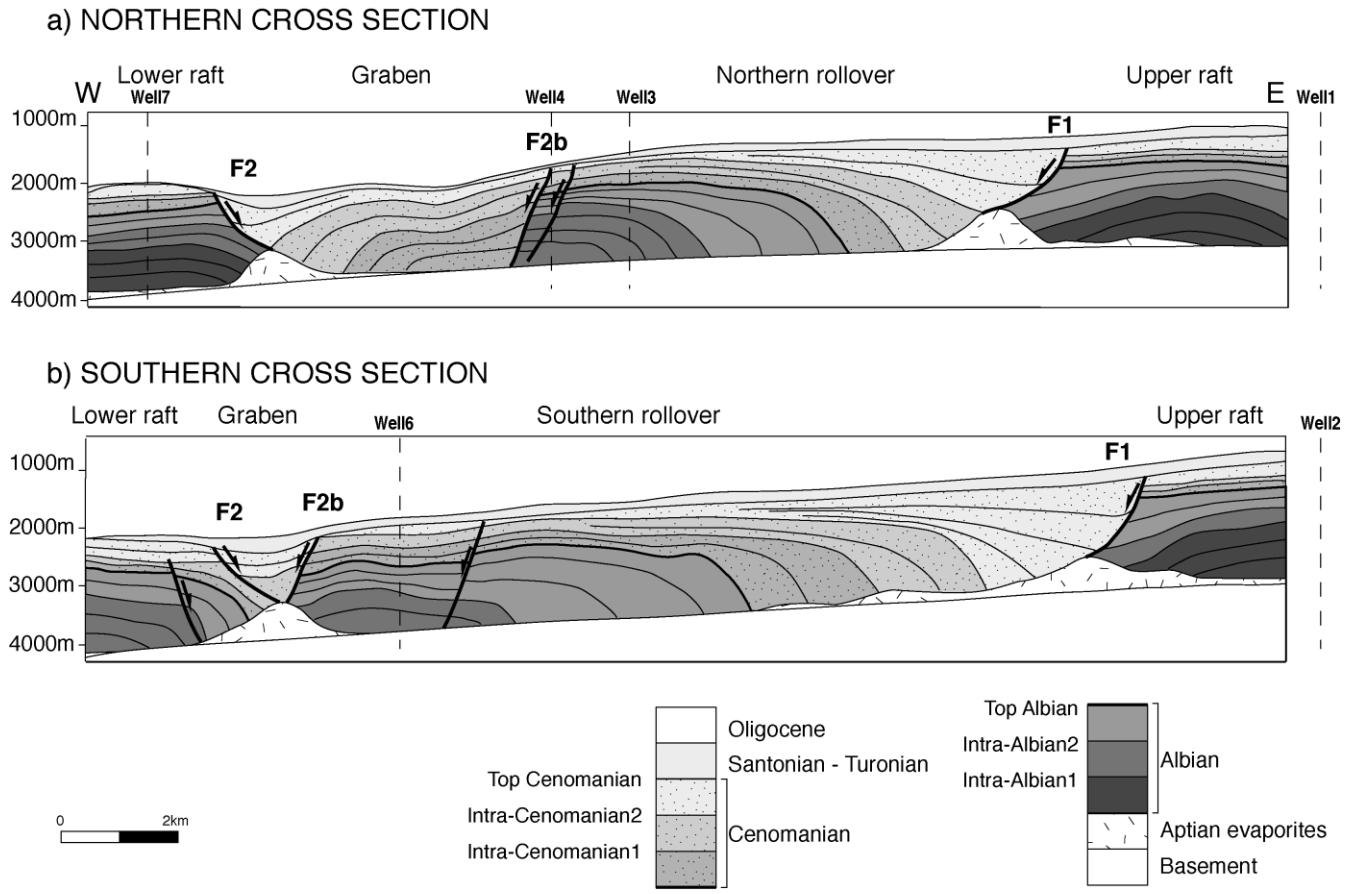

Fig. 4. Cross-sections in the 3-D geometrical model through the (a) northern and (b) southern rollovers. See location in Fig. 5.

facies and pre-littoral silts. During the Cenomanian, the system is dominated by detrital sedimentation coming from the east (Vernet et al., 1996).

The studied structure is composed of two rafts (with a core of Lower Albian sediments) separated by: (1) a main listric fault (F1) and its associated rollover anticline (involving Upper Albian and Cenomanian sediments), and (2) a graben involving Cenomanian sediments (Fig. 2). A time-converted 3-D seismic cube (20 km × 20 km, 12.5 m horizontal and 20 m vertical resolution) and data from nine wells (logs and cores) for calibration comprise the data base.

3. 3-D geometrical model

3.1. Construction

We interpreted 60 faults and seven stratigraphic horizons on seismic data: the top of the evaporites, two Albian horizons (Intra-Albian1 and Intra-Albian2), the top Albian, two Cenomanian horizons (Intra-Cenomanian1 and Intra-Cenomanian2) and the top Cenomanian.

We represented the folded and faulted stratigraphic horizons in 3-D, as irregular triangulated surfaces with gaps corresponding to fault cut-offs. We generated the triangulated surfaces and the fault cut-offs with the gOcad 3-D earth modeling software (Mallet, 1992) starting with the horizon and fault picks from 3-D seismic mapping and following the approach given in Rouby et al. (2000). The geometrical model was then depth converted using a vertical 1-D algorithm from average layer velocities calibrated at well locations. After depth conversion, the averaged velocities produced some discrepancies that we corrected by moving the horizon surfaces vertically to fit them at the well locations.

3.2. Structural analysis

Fig. 3 shows a perspective view of five stratigraphic horizons. We constructed two cross-sections through the northern and southern parts of the raft/listric fault system (Fig. 4) as well as isopach maps for the six time intervals (Fig. 5). Isopachs were measured perpendicularly to each top layer (not vertically).

Several structural units are identified in Figs. 4 and 5. The two rafts (upper and lower) show a core of Lower Albian (Figs. 4 and 5a). They are separated by, from east to west, a rollover anticline (composed of two sub-units) and a graben.

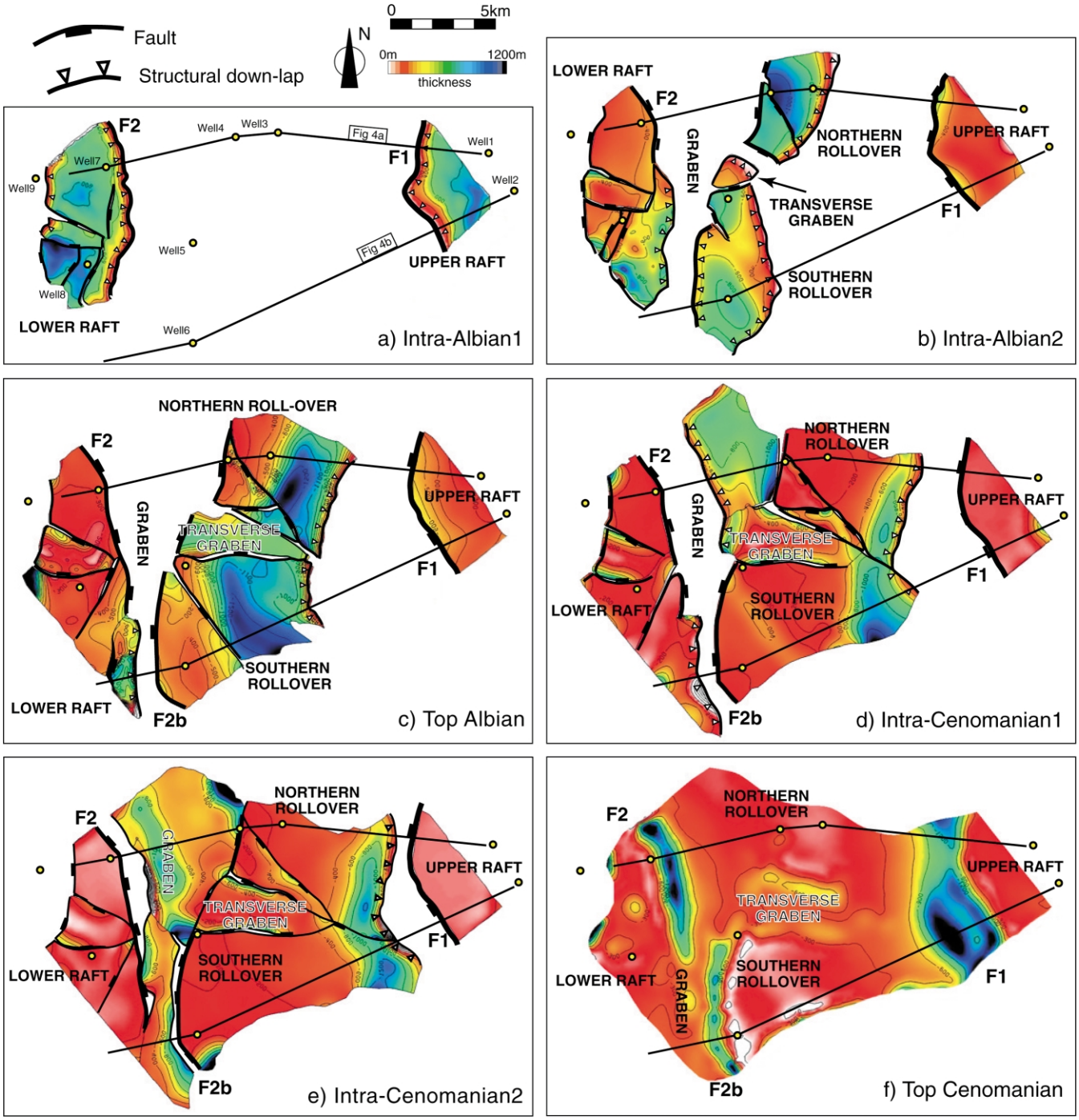

Fig. 5. Isopach maps showing the location of cross-sections and wells for the (a) Intra-Albian1, (b) Intra-Albian2, (c) Top Albian, (d) Intra-Cenomanian1, (e) Intra-Cenomanian2, and (f) Top Cenomanian horizons. Isopachs are measured perpendicularly to the top of each horizon.

The upper raft is bounded to the west by the main listric fault F1, dipping seaward, whereas the lower raft is bounded to the east by the listric fault F2, dipping landward (Fig. 4). These faults are composed of two segments, a brittle normal fault within the sedimentary overburden (separating the rollover and the upper raft) that curves and terminates downward as a shear zone in the décollement layer of evaporites (Mauduit and Brun, 1998).

In the footwall of both faults, the Intra-Albian1 layer is thinned by geometrical onlap/downlap against the evaporite rollers (Figs. 4 and 5a). Seismic data show that individual beds of the Intra-Albian1 show no significant changes in thickness as they approach their point of truncation against the evaporites. Upper Albian layers (Intra-Albian2 and Top Albian) thicken near these faults (Figs. 4 and 5a–c).

The rollover anticline involves Upper Albian and Cenomanian sediments and is bounded by F1 and F2b (antithetic with respect to F2; Figs. 4 and 5). In map view, it is

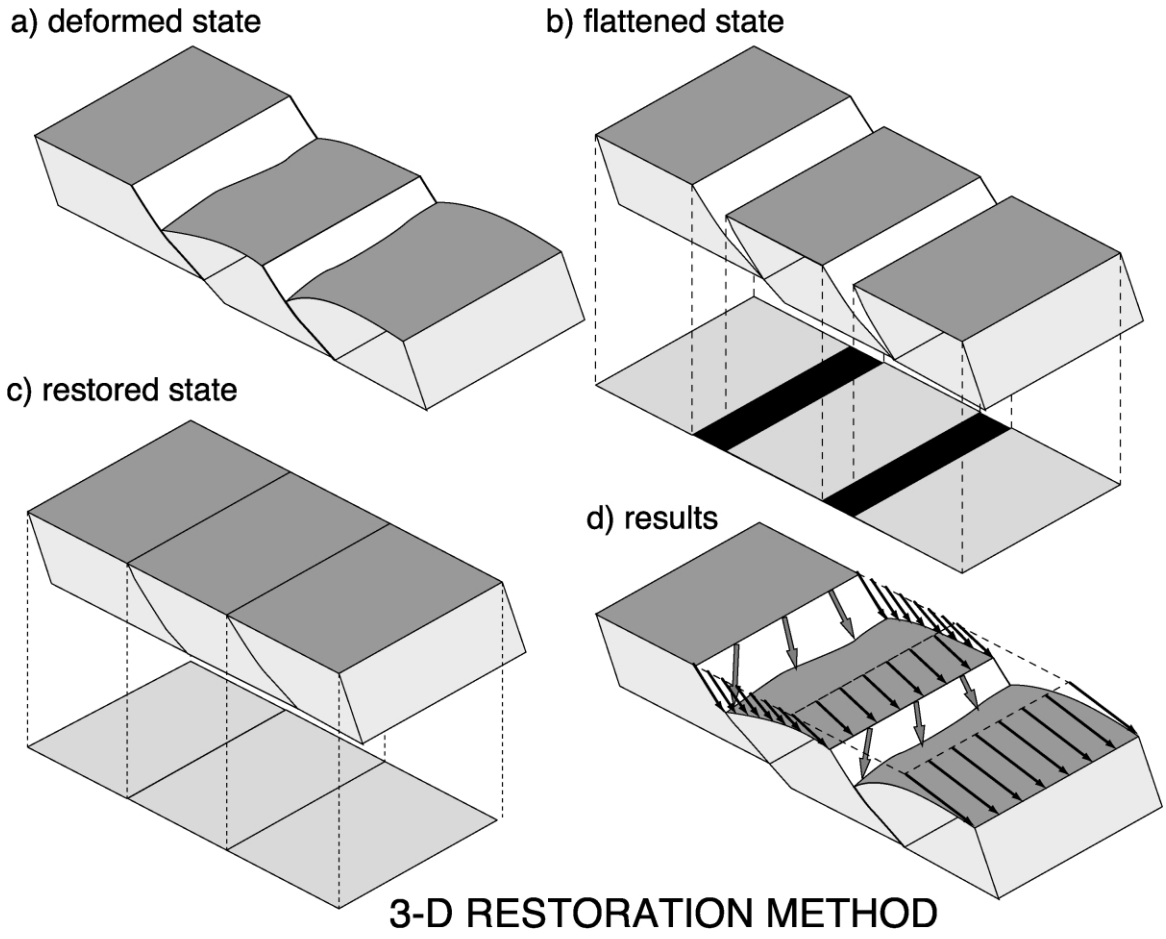

Fig. 6. Principle of the restoration method (after Rouby et al., 2000). (a) Initial data are made up of stratigraphic horizons represented by triangulated surfaces (surfaces composed of triangular elements, dark gray) that are offset by the faults (white surfaces). (b) Unfolding of the horizon. Normal faults appear as gaps separating fault compartments (black surface). (c) Unfaulting is then performed in map view. To invert the displacement on the faults, we close the fault gaps by rigid body displacement of the fault compartments. (d) The difference between the deformed and the restored state gives the 3-D finite displacement field (thin black arrows) and the directions of slip on the faults (thick gray arrows).

composed of two sub-units: the northern and southern rollovers separated by a transverse graben (Figs. 3 and 5). This transverse graben is perpendicular to the main faults, and approximately parallel to the expected principal direction of displacement. The graben results from a N–S component of extension probably produced by divergent directions of displacement between the northern and southern rollover units.

The graben involves Cenomanian sediments (Figs. 4 and 5d–f). It is bounded by a fault relay. To the north, a landward-dipping fault F2 relay with a seaward-dipping fault F2b to the south. This fault relays is particularly visible on the isopach maps of Intra-Cenomanian2 and Top Cenomanian (Fig. 5e and f).

The amount of displacement associated with F1 increases southward, whereas displacement increases northward for the faults bounding the graben (F2 and F2b; Fig. 5b–d). The spatial overlap between F1 and the faults bounding the graben (F2 and F2b) produces a ‘mock-turtle’ (e.g. Lower Albian units missing) anticline in between (Vendeville and Jackson, 1992a,b; Mauduit et al., 1997).

4. Restoration of the 3-D geometrical model

4.1. Method of 3-D surface restoration

The next step is to restore the stratigraphic horizons of the 3-D geometrical model. The restoration of a faulted and folded stratigraphic marker involves the numerical reconstruction of its undeformed geometry (Fig. 6).

Methods for unfolding 3-D surfaces have been recently proposed, based on two deformation mechanisms: flexural slip (i.e. surface area conservation; Gratier et al., 1991; Guillier, 1991; Gratier and Guillier, 1993; Samson, 1996; Williams et al., 1997) and homogeneous inclined shear (i.e. shear along vectors with constant inclination and direction; Kerr et al., 1993; Kerr and White, 1996). Commercial software are available to restore surfaces in 3-D based on the following approximations: (1) solving the restoration problem in 2-D cross-sections with interpolation between the sections, (2) limiting the number of faults, and (3) specifying the direction of slip on the faults, which is generally not known.

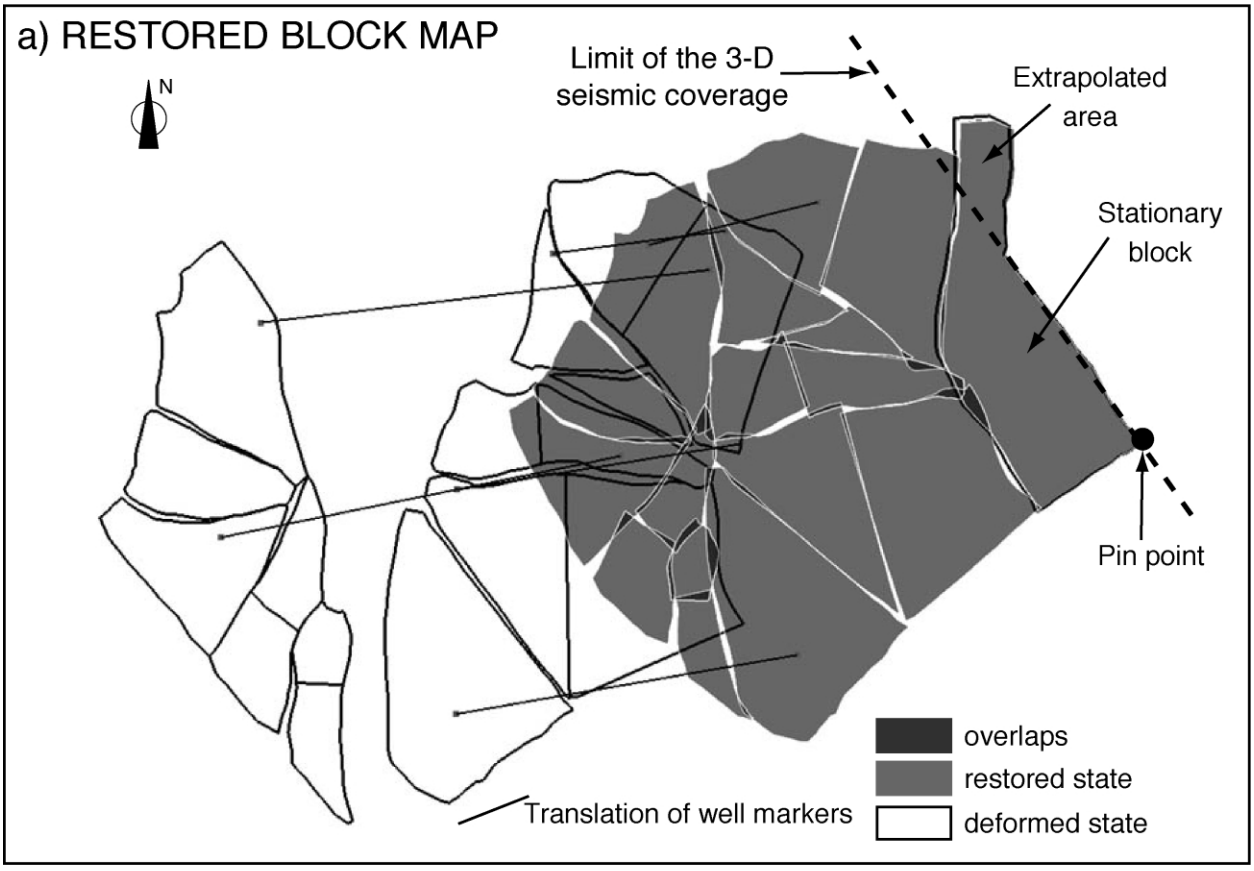
a) RESTORED BLOCK MAP
N
Limit of the 3-D seismic coverage
Extrapolated area
Stationary block
Pin point
overlaps
restored state
deformed state
Translation of well markers

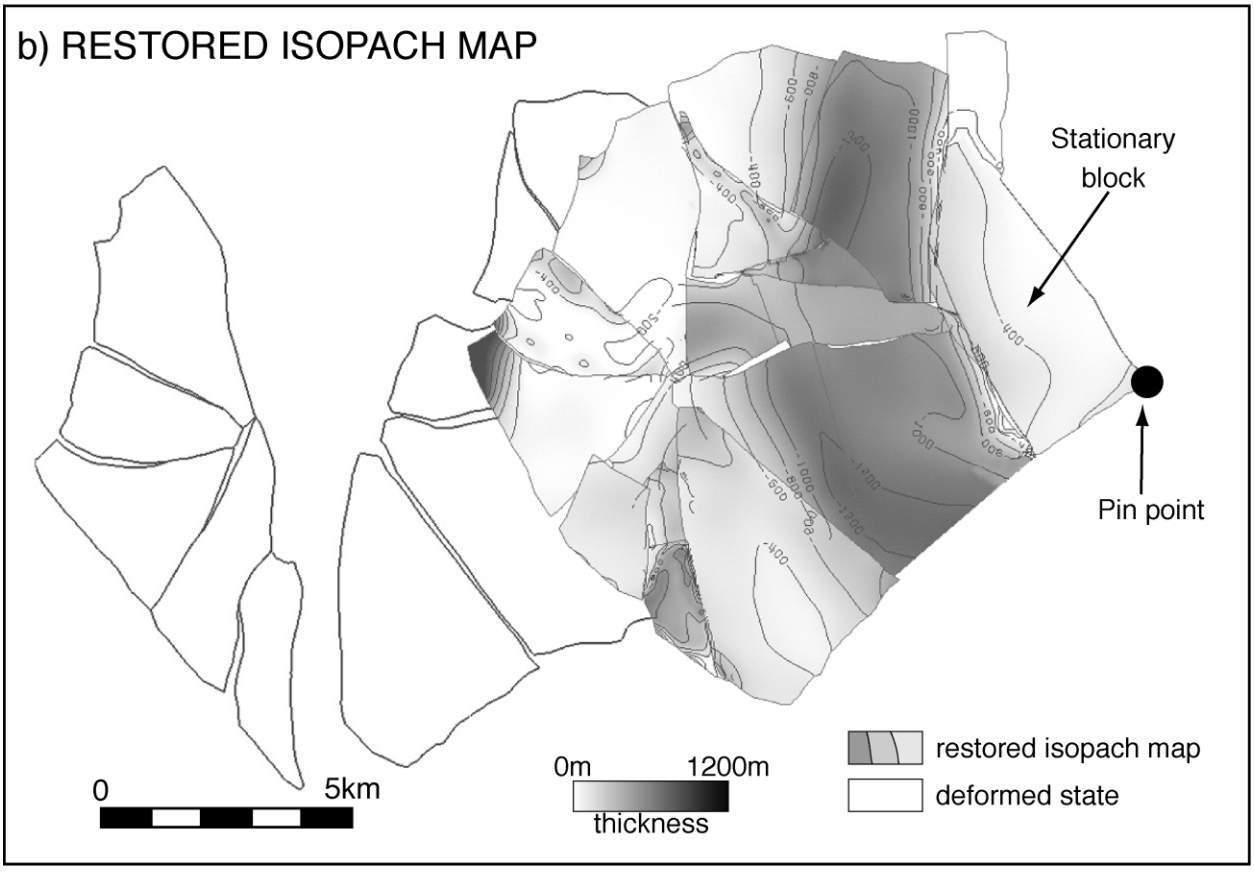
b) RESTORED ISOPACH MAP
Stationary block
Pin point
0
5km
0m
1200m
thickness
restored isopach map
deformed state

We chose the method of Rouby et al. (2000) to unfold and unfault 3-D surfaces because it allows the restoration of complex fault patterns and does not require a knowledge of the direction of slip on the faults. The main drawback of this approach is that it does not restore volumes, only sets of surfaces, each horizon being processed independently from the others.

We first unfold the surface using a finite (triangular) element approach (Fig. 6a and b). To do this, we assume that folding is accommodated either by flexural or inclined shear. We then invert the fault heave in map view (Fig. 6c), following the method of Rouby et al. (1993a). We assume rigid body behavior of the fault blocks (after the deformation associated with folding has been removed). The unfolded surface is carved up to obtain a map of fault-bounded blocks. We extrapolate fault traces and add artificial block boundaries to subdivide large and elongated blocks (Fig. 7a). A stationary block defines the displacement condition over part of the boundaries. The other blocks are packed against the stationary block using rigid body translations and rotations designed to minimize gaps and overlaps between blocks (Figs. 6c and 7b). When the best fit is obtained (area of gaps and overlaps is minimized) and is geometrically satisfactory (area of gaps and overlaps is negligible with respect to the area of blocks, i.e. less than 5%), we assume that the restored surface is the undeformed state of the horizon.

The difference between the deformed and restored state gives: the strain field associated with folding, the direction of displacement on the faults, and the 3-D finite displacement field associated with folding and faulting (Fig. 6d). By restoring several stratigraphic markers within the same structure, we may quantify the displacements for corresponding time increments.

A full discussion of the method (procedures, assumptions, boundary conditions, applicability, etc.) can be found in Rouby et al. (1993a,b, 2000). Here, we only summarize the results of these studies in terms of the sensitivity of the method to boundary conditions defined by the interpreter, including: (1) the unfolding mechanism, (2) the pin point used for unfolding and the stationary block(s) for unfaulting, and (3) the map of fault-bounded blocks.

The 3-D displacement fields related to different unfolding mechanisms (flexural or inclined shear, with varying shear angle for the latter) show a variability of less than 5% in vector length and 1% (less than 1°) in direction. This is because most of the displacement is usually accomplished extension on the faults.

The location of the stationary boundaries, whether for the unfolding step (pin point) or for the unfaulting step (stationary blocks) constrains the reference point used to compute the displacement fields. However, it does not significantly modify the strain maps (related to gradients of displacement) or the relative displacements between blocks.

The design of the block map is also shown to have little effect on the final 3-D displacement field (less than 2% in vector length and direction), providing elementary rules of fault extrapolation are followed. First, we extend fault traces until they meet other faults. Priority is given to the longest faults, with the assumption that they are the most active. Second, artificial block boundaries may be invoked to subdivide large and elongated blocks in order to allow for some internal deformation. Areas showing a poor fit between blocks in the first restoration attempts may help to pinpoint areas where these artificial boundaries are required to obtain a good fit (area of gaps and overlaps is negligible with respect to block surface, i.e. below 5%). Local dip anomalies corresponding to deformation zones (short wavelength folds or faults smaller than seismic resolution) may also be used to define these block boundaries.

4.2. Application to the 3-D model

We restored six stratigraphic horizons of the geometrical model (except the top of the evaporites). Indeed, evaporites probably do not deform according to the mechanisms assumed in the restoration method (flexural slip or inclined shear). The only information we obtained on the geometry of the evaporites layer is the topography of the base of the lower Albian (i.e. the top of the evaporites) from the reconstructed isopach maps (see below).

We unfolded the surfaces using inclined shear with shear vectors dipping at 75° from the horizontal and trending in a direction defined by the local dip of each triangle (the 'heterogeneous' inclined shear from Rouby et al. (2000)). This folding mechanism has given the best results in optimizing the unfolding mechanism of similar structures (Rouby et al., 2000).

The pin point for the unfolding was the southeastern corner of the upper raft (Fig. 7a). The unfolded surface was then subdivided to obtain a map of fault-bounded blocks (Fig. 7a). The upper raft (footwall of F1) was the stationary block for the unfaulting. The other blocks were packed against it, using rigid body translations and rotations designed to minimize gaps and overlaps between blocks (Fig. 7a). When the fit obtained was geometrically satisfactory, we assumed that the restored state was the undeformed state of the horizon.

To obtain a correct fit, we modified the block maps by extending the fault F1 to the north in an area not covered by 3-D seismic data (compare Figs. 5 and 7a). We also extended F1 in order to obtain a solution in which the

Fig. 7. Top view of the restoration of the Top Albian surface. (a) The block map of the deformed surface (thick black line) is first unfolded using the pin point as a stationary reference. The flattened surface is then unfaulted by packing the blocks against the stationary upper raft to give the restored surface (gray). The remaining gaps and overlaps (dark gray) between the blocks are about 3% of the initial surface. (b) Restored isopach maps of the Top Albian surface.

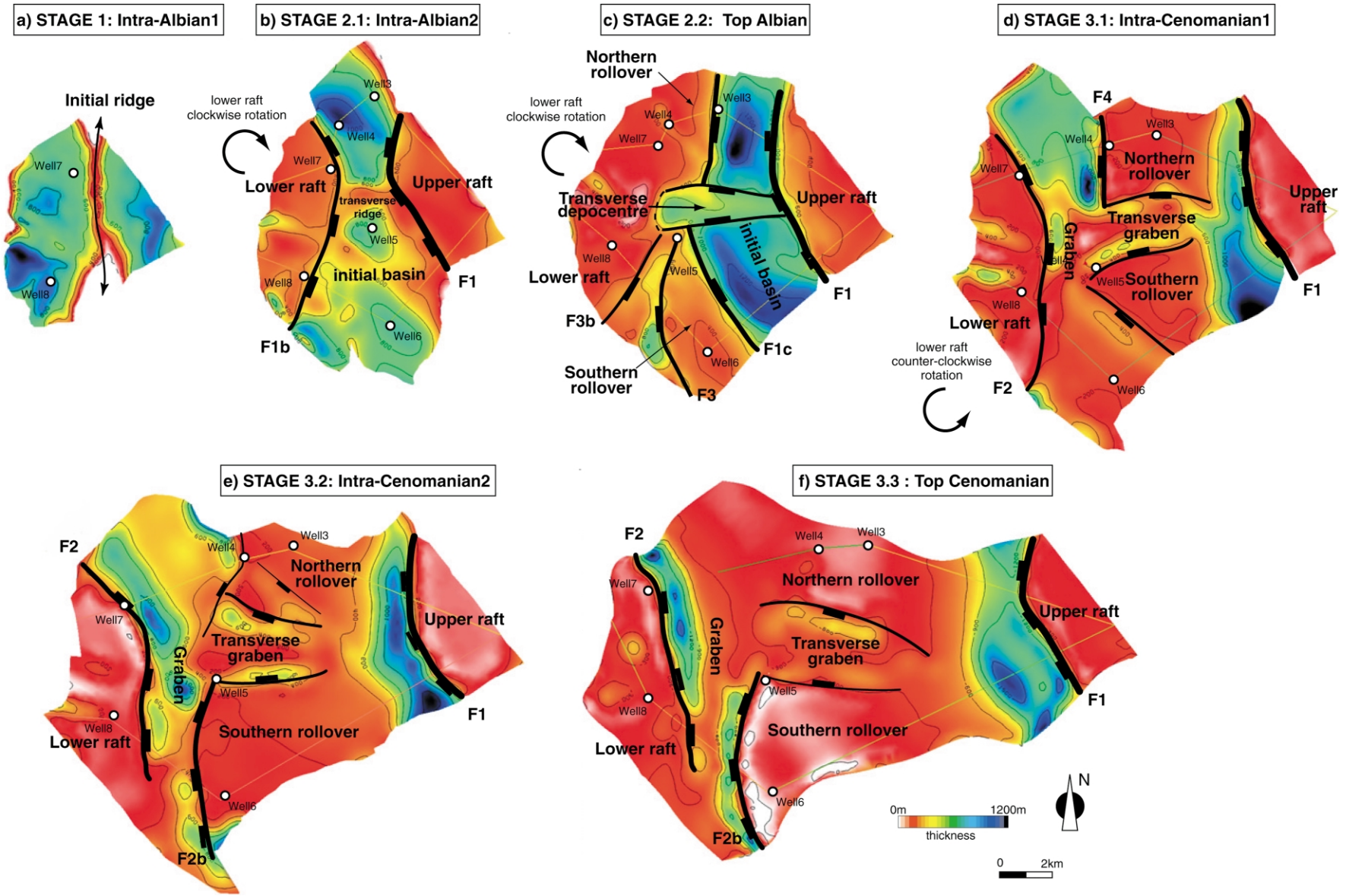

Fig. 8. Reconstructed isopach maps at the time of deposition of the top horizon (a) Intra-Albian1, (b) Intra-Albian2, (c) Top Albian, (d) Intra-Cenomanian1, (e) Intra-Cenomanian2, and (f) Top Cenomanian. Well locations are shown in the restored state in addition to the faults active during each time step. See text for explanation

southern corner of the upper raft matches the eastern corner of the southern rollover (Fig. 7a). This indirect constraint is determined by the geometry of the upper raft south of the 3-D seismic coverage. The southern boundary of the rollover in the 3-D model is actually a transfer fault, perpendicular to F1 and reaching the upper raft at the limit of the 3-D seismic data.

The difference between the deformed and restored states gave the 3-D finite displacement field associated with faults and folds. We applied this displacement field to the isopach maps (Fig. 7b) to retrieve their geometry in the restored state. Thus, by compiling the restoration of the six stratigraphic horizons, we reconstructed the geometry of the isopach maps at the time of deposition of the top of the six layers (reconstructed isopach maps; Fig. 8).

5. Reconstructed isopach maps

The reconstructed isopach maps show the evolution of the 3-D geometry of the fault system (Fig. 8). Because we do not actually restore the fault surfaces, the faults shown on these maps are interpreted from the geometry of the depocentres after reconstruction. We assume that thickened areas indicate faults that are active during the time step corresponding to the isopach interval. The dip of the faults is determined from the asymmetry of the depocentres.

Some faults (e.g. F1) remain active throughout the evolution of the system (we use the same name on all maps), but others only during some time increments (see F5 on Fig. 8d). Some faults may have been reactivated (e.g. F4 may be the same structure as F2b). However, because we could not be sure, we gave such faults different names. Therefore, some of the faults could not be shown on cross-sections or maps of the current state.

5.1. Albian: Intra-Albian1, Intra-Albian2 and Top Albian

At the end of Intra-Albian1, two depocentres of Lower Albian sediments (that later become the raft units) were separated by a very thin N–S band of sediments trending N–S and corresponding to an initial ridge (Fig. 8a).

At the end of Intra-Albian2, depocentres migrated from the rafts to a N–S trending basin at the location of the ridge during the previous stage (initial basin: area including Wells 3–6 on Fig. 8b). The northern depocentre was narrower with thicker deposits than the southern depocentre. They were separated by a thinner band of sediments trending E–W, corresponding to a transverse ridge. Rafts were separated by 3 km in the north and 5 km in the south. Although we show faults bounding the N–S depocentre (F1 and F1b on Fig. 8b), its boundaries with the rafts are not very sharp and these faults might not actually have been formed at that stage.

At the end of the Albian, rafts were separated by a distance of about 5 km in the north and 7 km in the south (Fig. 8c). The N–S depocentre (initial basin) remained located immediately to the west of the upper raft, whereas the area around Wells 3–6 (rollover units) was translated to the east and showed a small thickness of preserved sediments. Some sediments are preserved between the southern rollover and the lower raft (faults F3 and F3b). The transverse ridge became a transverse depocentre separating the initial basin into a northern and a southern part. At that time, the eastern and western boundaries of the initial basin were sharper and probably corresponded to a normal fault (F1 and F1c).

5.2. Cenomanian: Intra-Cenomanian1, Intra-Cenomanian2 and Top Cenomanian

At the end of Intra-Cenomanian1, the main depocentre was asymmetric (narrowing northward) and associated with F1 (Fig. 8d). Another important asymmetric depocentre formed between the northern rollover unit and the lower raft (fault F4, dipping seaward, developing between Wells 4 and 7). Sediments were also preserved next to the faults bounding the transverse depocentre that became the transverse graben. At that stage, the rafts were separated by more than 8 km (Fig. 8d).

The present-day structure was acquired during the Intra-Cenomanian2 and Top Cenomanian (Fig. 8e and f). Two main areas of sediment preservation are identified. As during the previous stage, the first one is asymmetric, narrowing northward and associated with F1. The second, located between the northern rollover and the lower raft, is composed of two asymmetric depocentres: along the lower raft to the north (F2) and along the southern rollover unit to the south (F2b). The transverse graben was still active at this time. Rafts were separated by about 12 km at the end of Intra-Cenomanian2 and 16 km at the Top Cenomanian (Fig. 8e and f).

6. Discussion

6.1. Model of evolution of the fault system

The reconstruction of the successive 3-D geometries of the fault system allows us to propose a model of evolution involving three main stages corresponding to the (1) Lower Albian, (2) Upper Albian, and (3) Cenomanian.

The ridge separating the two depocentres during the Lower Albian (Fig. 8a) can be interpreted as an evaporite wall. Its growth may be related to the stretching of the sedimentary cover by regional extension forming two rafts of Intra-Albian1 sediments and allowing the rise of an evaporite wall. Note that our restoration of the Lower Albian stage does not take into account the potential width of this wall.

Stretching of the Intra-Albian1 cover may have occurred either (1) during the deposition of the Lower Albian sediments (Intra-Albian1 sediments are syn-kinematic) or (2) after deposition of the Lower Albian (Intra-Albian1 sediments are pre-kinematic). In the first case, deposited sediments were immediately stretched while forming the rafts by down-

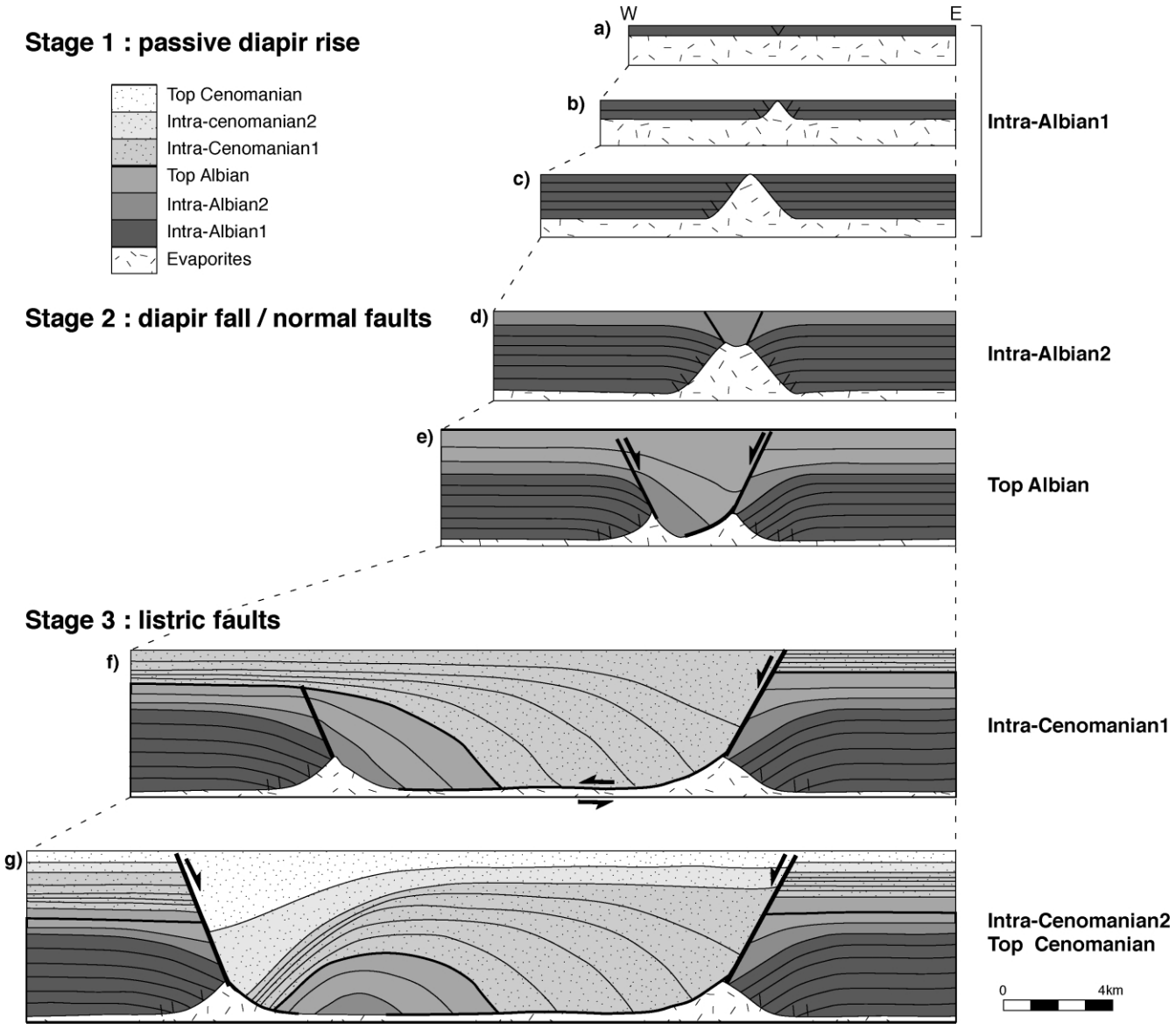

Fig. 9. Evolution of the raft/listric fault system in three stages. (a–c) During Stage 1 (Intra-Albian1), an initial diapir rises passively as sediments are stretched by regional extension and the upper and lower rafts are built down. (d) In Stage 2 (Intra-Albian2 and Top Albian), the diapir sags as extension continues. (e) This subsiding area evolves into a graben, bounded by normal faults, becoming progressively asymmetric. (f) During Stage 3 (Top Albian through Top Cenomanian) the graben evolves into a large listric fault and its associated rollover. (g) Later (Intra-Cenomanian1 through Top Cenomanian), the lower raft is separated from the rollover unit by the graben and, consequently, the rollover forms a 'mock-turtle' anticline.

building (Vendeville and Jackson, 1992a). The Intra-Albian1 layer should terminate by onlap/downlap against the evaporite rollers and show no or little deformation (Fig. 9a–c). In the second case, stretching of the sedimentary cover formed fault zones that localized and initiated the rise of the diapirs through their structurally thinned floor (Vendeville and Jackson, 1992a). The Intra-Albian1 layer should then be thinned by faulting near the salt diapir. As pointed out earlier, seismic data show that, in the footwall of F1 and F2 (i.e. on both sides of the initial salt wall) the Intra-Albian1 layer terminated by onlap/downlap against the evaporite rollers and not by faulting (Fig. 2). For this reason, we prefer to interpret the Intra Albian1 as a syn-kinematic layer (Fig. 9a–c).

During both stages of the Upper Albian (Fig. 8b and c), the migration of depocentres above the salt wall shows that it became a subsiding area in which sediments were preserved (initial basin). This symmetric depocentre can be observed on cross-sections as the thickening of Upper Albian layers in the footwall of F1 and F2 (Figs. 2 and 4). This geometry can be interpreted as the result of regional extension bringing the rafts farther apart. The subsiding area located above an evaporite wall can be associated with two different phases in the development of the salt wall during ongoing extension. The initial basin was contemporaneous with the reactive rise of the evaporite wall through

the structurally thinned Lower Albian sediments (Vendeville and Jackson, 1992a; Nalpas and Brun, 1993). In this case, extension initiated during the deposition of Upper Albian. Alternatively, the initial basin was contemporaneous with the falling phase of the evaporite wall as the evaporite supply to the diapir was depleted so that it sagged as it widened (Vendeville and Jackson, 1992b). In this case the extension initiated during the deposition of the Lower Albian sediments. As discussed above, we favor the interpretation of Intra-Albian1 as a syn-kinematic layer; that is to say, the initial basin formed during the falling phase of the salt wall (Fig. 9d and e).

At the Albo–Cenomanian boundary, the geometry of the fault system changed significantly. The single symmetric depocentre (initial basin) is replaced by two asymmetric depocentres associated with faults. This geometry indicated that, throughout the Cenomanian, regional extension was accommodated by two main fault systems: the main fault F1 and a new fault system developing between the rollover units and the lower raft (Fig. 9f and g). The new fault system initiated during the Intra-Cenomanian1 as a seaward-dipping fault (fault F4; Fig. 8d). During Intra-Cenomanian2 and Top Cenomanian, faulting developed farther southward and formed a graben bounded by a fault relay (F2 and F2b). It eventually separated the lower raft from the rollover units (Figs. 8e and f and 9f and g).

Analog modeling has shown that, within gravitational extension domains, normal faults usually initiate as planar surfaces, and become progressively listric as faulting, rotation about an horizontal axis, and sedimentation interact (Vendeville and Cobbold, 1988; Mauduit and Brun, 1998). The resulting surfaces are composed of a brittle normal fault within the sedimentary overburden that transitions into a shear zone as it curves and terminates downward in the décollement layer (Mauduit and Brun, 1998). Accommodation of displacement along a listric surface results in the development of a rollover anticline within the hanging wall.

The change of geometry of the initial basin at the end of the Albian (Fig. 8c and d) is interpreted as the transition between a system of planar faults bounding a symmetric basin that evolves into an asymmetric basin as F1 becomes the main fault (Fig. 9e and f). The area around Wells 3–6 becomes a subsiding area. The main subsiding area remains next to the more steeply dipping part of the fault surface (Figs. 8c–f and 9e and f).

The evolution of the growth fault/raft system can therefore be described as the progressive separation of two rafts by regional extension, resulting in the development of an intervening basin that evolved in different stages (Fig. 10): (1) the rise of an evaporite wall during the Lower Albian, (2) the development of a symmetric basin as the evaporite wall is reduced and buried, and (3) the development of asymmetric basins related to two systems of listric faults. The initial salt wall is only preserved as salt rollers in the footwall of F1 and F2 (Figs. 4 and 9g).

6.2. 3-D evolution and timing of faults

The reconstruction of the successive 3-D geometries allows us to describe the growth of this fault system in 3-D and to identify the incremental steps of its deformation.

The transverse ridge evolving into a depocentre and graben (Fig. 8) indicates that, very early in the history of the structure (Intra-Albian1), regional E–W extension was associated with a N–S component of extension. The global 3-D displacement field was thus divergent in map view (20° maximum), resulting in a state of non-planar bulk strain.

During both stages of the Upper Albian (Fig. 8b and c), the geometry of the system (widening of the initial basin southward during Intra-Albian2, development of F3 and F3c during Top Albian) indicates a displacement between the two rafts that increases from north to south. The seaward translation of the lower raft is therefore associated with a finite rotation by about 10° clockwise of the lower raft about a vertical axis (rotation of the line joining Wells 7 and 8 between Intra-Albian1 and Top Albian). During the Intra-Cenomanian1, the new fault system forming between the rollover units and the lower raft (F4) results in a counter-clockwise rotation about a vertical axis of the lower raft that brings it back into a N–S position (bearing of the line joining Wells 7 and 8; Fig. 8d–f).

The rollover units are located between the two fault systems (the main fault F1 and the faults bounding the graben). Consequently, they display a mock-turtle anticline structure (Vendeville and Jackson, 1992a,b; Mauduit et al., 1997; Figs. 4 and 9g). Because of the timing of faulting (F1 formed during the Upper Albian, the graben during the Cenomanian), the mock-turtle anticline is asymmetric (Vendeville and Jackson, 1992a,b; Mauduit et al., 1997; Figs. 4 and 9g).

7. Conclusions

Using a new approach of 3-D restoration, this study has shown how it is possible to determine: (1) the processes of deformation of a fault system, (2) its kinematics and (3) the incremental steps of deformation.

We reconstruct the evolution of the growth fault/raft system in 3-D and show that it can be described as the progressive separation of two rafts by regional extension, resulting in the development of a basin in between that evolved in three main stages: (1) the rise of an evaporite wall during the Lower Albian, (2) the development of a symmetric basin as the diapir was reduced and buried during the Upper Albian, and (3) the development of asymmetric basins related to two systems of listric faults during the Cenomanian.

Some important features of the growth fault/raft system can only be observed in 3-D:

1. The rollover anticline (associated with the main fault F1) is composed of two sub-units separated by an E–W oriented transverse graben.

2. The displacement field is divergent in map view, resulting in a state of non-planar bulk strain.
3. The rollover units are located within the overlap area of two fault systems (the main fault and the graben) and, therefore, display a mock-turtle anticline structure.
4. The graben is bounded by a fault relay.

Other important features could only be observed with increments of deformation. The seaward translation of the lower raft is associated with two successive rotations in opposite sense (clockwise then counter-clockwise). The rotation is due to the two main fault systems developing successively. The main listric fault F1 (to the east) formed during the Upper Albian, and the faults-bounding graben (to the west) during the Cenomanian.

Acknowledgements

We are grateful to Elf Congo for financial support of this study and providing us with the data set, as well as Elf EP for technical support. We acknowledge Peter Cobbold for improving the manuscript. Ken Fowler, Mike Hudec and Ted Apotria provided very detailed and stimulating reviews, and Mike Carpenter improved the English style.

References

Burollet, P.F., 1975. Tectonique en radeaux en Angola. Bulletin de la Société Géologique de France XXII, 503–504.

Cowie, P.A., 1998. Normal fault growth in three-dimensions in continental and oceanic crust. In: Buck, W.R., Delaney, P.T., Karson, J.A., Lagabrielle, Y. (Eds.), Faulting and Magmatism at Mid-Ocean Ridges. Geophysics Monograph 106, pp. 325–347.

Curie, D., 1984. Ouverture de l'Atlantique Sud et discontinuité intraplaque: une nouvelle analyse. Ph.D. thesis, University of Brest.

Duval, B., Cramez, C., Jackson, M.P.A., 1992. Rafts tectonics in the Kwanza Basin, Angola. Marine and Petroleum Geology 9, 389–404.

Gratier, J.P., Guillier, B., 1993. Compatibility constraints on folded and faulted strata and calculation of total displacement using computational restoration (UNFOLD program). Journal of Structural Geology 15, 391–402.

Gratier, J.P., Guillier, B., Delorme, A., Odonne, F., 1991. Restoration and balanced cross section of a folded and faulted surface by computer program: principle and application. Journal of Structural Geology 13, 11–115.

Guillier, B., 1991. Dépliage automatique de strates plissées et faillées: application à l'équilibrage des structures naturelles. Ph.D. thesis, University of Grenoble.

Kerr, H., White, N., 1996. Application of an inverse method for calculating three dimensional fault geometries and slip vectors, Nun River field, Nigeria. American Association of Petroleum Geologist Bulletin 80, 432–444.

Kerr, H., White, N., Brun, J.P., 1993. An automatic method for determining three-dimensional normal fault geometry. Journal of Geophysical Research 98, 17837–17857.

Liro, L.M., Coen, R., 1995. Salt deformation history and postsalt structural trends, offshore southern Gabon, west Africa. In: Jackson, M.P.A., Roberts, D.G., Snelson, S. (Eds.), Salt Tectonics: a Global Perspective. American Association of Petroleum Geologist Memoir 65, pp. 323–331.

Lundin, E.R., 1992. Thin-skinned extensional tectonics on a salt detachment, northern Kwanza Basin, Angola. Marine and Petroleum Geology 9, 405–411.

Mallet, J.L., 1992. Discrete smooth interpolation in geometric modelling. Computer Aided Design 24, 178–191.

Mauduit, T., Brun, J.P., 1998. Growth fault/rollover systems: birth, growth and decay. Journal of Geophysical Research 103, 18119–18136.

Mauduit, T., Gaullier, V., Guerin, G., Brun, J.P., 1997. On the asymmetry of turtle-back growth anticline. Marine and Petroleum Geology 14, 731–762.

Merle, O., Abidi, N., 1995. Approche expérimentale du fonctionnement des rampes émergentes. Bulletin de la Société Géologique de France 166, 439–450.

Nalpas, T., Brun, J.P., 1993. Salt flow and diapirism related to extension at crustal scale. Tectonophysics 228, 349–362.

Nalpas, T., Györfi, I., Guillocheau, F., Lafont, F., Homewood, P., 1999. Influence de la charge sédimentaire sur le développement d'anticlinaux synsédimentaires. Modélisation analogique et exemple de terrain (bordure sud du bassin de Jaca). Bulletin de la Société Géologique de France 170, 733–740.

Rouby, D., Cobbold, P.R., Szatmari, P., Demercian, S., Coelho, D., Rici, J.A., 1993a. Least-squares palinspastic restoration of regions of normal faulting. Application to the Campos basin (Brazil). Tectonophysics 221, 439–452.

Rouby, D., Cobbold, P.R., Szatmari, P., Demercian, S., Coelho, D., Rici, J.A., 1993b. Restoration in plan view of faulted Upper Cretaceous and Oligocene horizons and its bearing on the history of salt tectonics in the Campos Basin (Brazil). Tectonophysics 228, 435–445.

Rouby, D., Suppe, J., Xiao, H., 2000. 3-D restoration of complexly faulted and folded surfaces using multiple unfolding mechanisms. American Association of Petroleum Geologist Bulletin 84, 805–829.

Samson, P., 1996. Equilibrage de structures géologiques 3-D dans le cadre du projet GOCAD. Ph.D. thesis, Institut National Polytechnique de Lorraine.

Spathopoulos, F., 1996. An insight on salt tectonics in the Angola basin, South Atlantic. In: Alsop, G.I., Blundel, D.J., Davison, I. (Eds.), Salt Tectonics. Geological Society of London Special Publication 100, pp. 153–174.

Tondji-Biyo, J.J., 1995. Chevauchements et bassins compressifs: influence de l'érosion et de la sédimentation. Modélisation analogique et exemples naturels. Mémoires de Géosciences Rennes 59, Rennes.

Vendeville, B., Cobbold, P.R., 1987. Glissements gravitaires synsédimentaires et failles normales listriques: modèles expérimentaux. Comptes Rendus de l'Académie des Sciences de Paris 305, 1313–1319.

Vendeville, B., Cobbold, P.R., 1988. How normal faulting and sedimentation interact to produce listric fault profiles and stratigraphic wedges. Journal of Structural Geology 10, 649–659.

Vendeville, B.C., Jackson, M.P.A., 1992a. The rise of diapirs during thin skinned extension. Marine and Petroleum Geology 9, 331–353.

Vendeville, B.C., Jackson, M.P.A., 1992b. The fall of diapirs during thin skinned extension. Marine and Petroleum Geology 9, 354–371.

Vendeville, B., Cobbold, P.R., Davy, P., Brun, J.P., Choukroune, P., 1987. Physical models of extensional tectonics at various scales. In: Coward, M.P., Dewey, J.F., Hanckock, P.L. (Eds.), Continental Extensional Tectonics. Geological Society of London Special Publication 28, pp. 95–107.

Vernet, R., Assoua-Wande, C., Massamba, L., Sorriaux, P., 1996. Paléogéographie du Crétacé (Albien–Maastrichtien) du bassin côtier congolais. Mémoires du Bulletin des Centres de Recherche et d'Exploration-Production de Elf 16, 39–55.

Williams, G.D., Kane, S.J., Buddin, T.S., Richards, A.J., 1997. Restoration and balance of complex folded and faulted rock volumes: flexural flattening, jigsaw fitting and decompaction in 3-D. Tectonophysics 273, 203–218.